Dynamics of colliding ultracold plasmas

J. P. Morrison and E. R. Grant

Phys. Rev. A **91**, 023423 — Published 20 February 2015

DOI: 10.1103/PhysRevA.91.023423

Dynamics of colliding ultracold plasmas

J. P. Morrison and E. R. Grant*
Department of Chemistry, University of British Columbia, Vancouver, BC V6T 1Z3, Canada

Formation of a secondary plasma of NO^+ ions and electrons within an ultracold plasma produces an observable change in the hydrodynamics of the system. Direct photoionization adds energetic electrons, which increase the rate of expansion. The introduction of a secondary Rydberg gas has the opposite effect. In both cases, the added ions create an inertial drag that acts initially to retard the expansion of the electron gas. A cold-ion hydrodynamic shell model, which accounts well for the effect of energy added by photoionization electrons, predicts the formation of collisionless shock waves.

PACS numbers: 52.55.Dy, 32.80.Ee, 33.80.Gj, 34.80.Lx

I. INTRODUCTION

The free expansion of a plasma directly reflects its internal kinetic energy. In the very simple limit of a spherical Gaussian ion/electron density distribution, a self-similar solution of the Vlasov equations describes the hydrodynamics of such expansions analytically [1].

Experiments that explore the interaction of two such systems offer an elementary test bed on which to explore the complex microphysics of colliding plasmas [2, 3], and a scaleable simulator to aid in understanding the dynamics of high-energy laboratory [4, 5] and natural systems [6].

For an ultracold plasma, where ions have energies less than a few degrees Kelvin, the rate of expansion depends largely on the temperature of the electron gas [1]. The electron temperature of a plasma is of great interest, because it determines the magnitude of the electron correlation parameter, $\Gamma_e = e^2/(4\pi\epsilon_0 a_{ws} k_B T_e)$, where the Wigner-Seitz radius, a_{ws}, relates to density by, $a_{ws} = \sqrt[3]{3/4\pi\rho}$. A $\Gamma_e > 1$ signifies strong coupling.

Hydrodynamic models for the expansion of Gaussian ultracold plasmas created by threshold ionization at the $\sim 10^9$ cm^{-3} density of a magneto-optical trap (MOT), conform with experimental electron temperatures greater than 30 K [7], and $\Gamma_e < 1$.

The evident heating of electrons in these systems accords with the expected energy transfer kinetics associated with coupled rate processes of three-body recombination and collisional relaxation of neutrals by electron impact [8].

Plasmas formed in supersonic molecular beams at orders of magnitude higher density exhibit slower expansion suggesting lower electron temperature [9–12]. These results do not square with classical MD simulations, which hold that correlation heating alone suffices to limit Γ_e to values smaller than 0.5 [13, 14].

This begs two questions: Do the ions formed at the density of a molecular beam ultracold plasma undergo a conventional ambipolar expansion driven by the electron gas? Does the kinetic energy of this electron gas fit with the temperature suggested by the observed rate of this expansion?

In the present work, we attempt to address these questions by exploring the responsiveness of a molecular beam ultracold plasma to interventions that perturb the electron temperature and alter the radial velocity distribution of the expanding ions. In effect, we use secondary laser excitation to create a plasma expanding within a plasma.

In our experiment, double-resonant excitation first excites a small fraction of the NO molecules in a selected volume of a seeded supersonic molecular beam to produce a Rydberg gas, $|n_0>$, which evolves to form an ultracold plasma. A second pair of lasers intercepts the same volume 10 μs later. Depending on chosen laser wavelengths, this secondary excitation either ionizes residual ground-state NO, injecting a distribution of stationary ions and hot electrons, or creates a secondary Rydberg gas within the volume of the original plasma.

Unsurprisingly, these interventions change the observed expansion behaviour of the plasma. We develop a hydrodynamic, plasma-in-plasma model to explain our observations. This model both accounts for the effects of perturbation, and serves to solidify our interpretation of the unperturbed expansion.

II. EXPERIMENTAL

The experiment seeds nitric oxide at 10 percent in a pulsed jet of helium. The skimmed expansion from a stagnation pressure of 5 atm through a 0.5 mm nozzle forms a supersonic molecular beam in which NO in the interaction volume, 10 cm downstream, has a density of 10^{13} cm^{-3} and a laboratory velocity of 1400 m s^{-1}. In the moving frame, the entrained NO has a longitudinal temperature of $T_\parallel \approx 500$ mK, and a transverse temperature, $T_\perp$, at least 10 times smaller.

Double resonant excitation pulses from a pair of tuneable dye lasers, ω_1 and ω_2, promotes about 12 percent of the ground-state NO in the interaction volume to a selected high Rydberg state. Tuning ω_1 to 44199 cm^{-1},

*Author to whom correspondence should be addressed. Electronic mail: edgrant@chem.ubc.ca

a pulse energy of 80 μJ, saturates the transition from the negative parity lambda doublet component of the NO $X\ ^2\Pi\ N'' = 1\ (J = 1/2)$ to the positive parity $A\ ^2\Sigma^+\ N' = 0\ (J = 1/2)$ state. Then, with ω_2 tuned to 30490 cm^{-1}, a pulse energy of 12 mJ saturates a second optical transition, forming a Rydberg gas with $n_0 = 50$ in the f series converging to $N^+ = 2$, designated $50f(2)$.

Coupled rate simulations according with time-resolved pulsed-field ionization experiments suggest that this dense Rydberg gas evolves to plasma on the timescale of tens of nanoseconds [15].

Figure 1 diagrams the experimental apparatus. We monitor the growing width of the plasma as it transits a detection plane formed by a moveable grid, G_2, that intercepts the interaction volume propagating on the axis of the molecular beam. The longitudinal position of the G_2 detection assembly determines the propagation time of the plasma through the field-free region between the entrance aperture, G_1, and the detection plane.

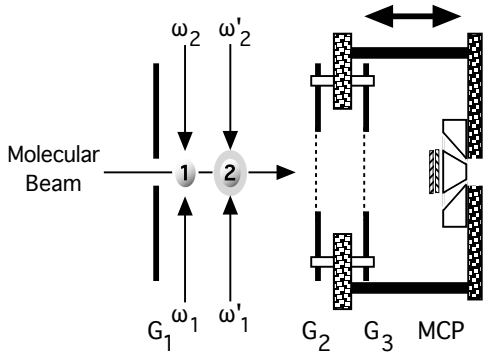

FIG. 1: Experimental apparatus. A skimmed supersonic molecular beam enters a nominally field-free region through an aperture in grid G_1. There it intersects counter-propagating laser beams indicated as ω_1 and ω_2. Downstream, laser pulses, ω_1' and ω_2', timed to intercept the the initially excited volume, excite residual ground state NO. As the excitation volume transits the plane defined by grid G_2, a microchannel plate detector (MCP) situated behind grid G_3 collects the signal of extracted plasma electrons. The carriage holding G_2, G_3 and the MCP detector translates in vacuum within a 20 cm interval under stepper motor control.

As the plasma travels in z through the G_2 detection plane, dislodged electrons produce a Gaussian signal waveform. The width of this waveform in time gauges the radius of the plasma charge distribution in the y, z plane. This radius grows with time as the plasma expands.

We perturb this plasma by intercepting the interaction volume with overlapped, co-propagating laser beams, ω_1' and ω_2', 14 mm downstream from the point of initial excitation. With pulse energy on the order of 100 μJ, ω_1' serves again to saturate the transition from the residual ground-state NO $X\ ^2\Pi\ N'' = 1\ (J = 1/2)$ to the $A\ ^2\Sigma^+\ N' = 0\ (J = 1/2)$ state.

Setting ω_2' to reach an energy above the double-resonant ionization threshold of NO drives this A-state population into the continuum of NO^+ ions and free electrons. Tuning ω_2' to a resonance below threshold prepares a secondary Rydberg gas. We use the comparative signal produced by $\omega_1' + \omega_2'$ to optimize the alignment of the second pair of lasers on the active plasma.

III. RESULTS

When the two pairs of lasers excite separate volumes of NO propagating along the axis of the molecular beam, we observe the electron-signal waveforms of two interaction volumes transiting G_2. As shown in Figure 2, these waveforms coalesce when pulses, ω_1' and ω_2', incident at position 2 arrive at the delay time required to intercept the plasma volume created at position 1 by $\omega_1 + \omega_2$.

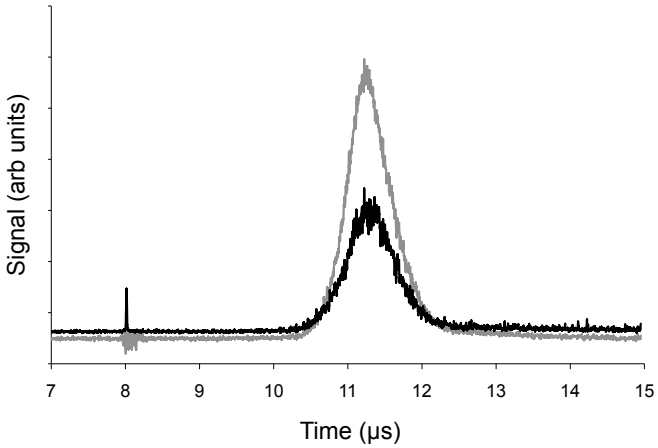

FIG. 2: Black trace: Waveform observed when the illumination volume formed by laser pulses, $\omega_1 + \omega_2$ at position reaches the detection grid, G_2. Grey trace: Typical waveform observed when laser pulses $\omega_1' + \omega_2'$ intercept this volume at position 2.

We determine how the plasma expands as a function of time by fitting Gaussian functions to the electron signal waveform detected at successive positions of G_2. Figure 3 plots the RMS radius as a function of flight time for an unperturbed plasma compared with that observed for plasmas perturbed either by (1) setting ω_2' to the above threshold energy of 30,590 cm^{-1}, which adds a hot electron component with an excess energy of 55 cm^{-1} or (2) setting ω_2' to the below-threshold energy of 30,504 cm^{-1}, which creates a $60f(2)$ Rydberg gas within the original plasma volume.

IV. DISCUSSION

The central curve in Figure 3 describes the free expansion of the simple plasma that evolves solely from a

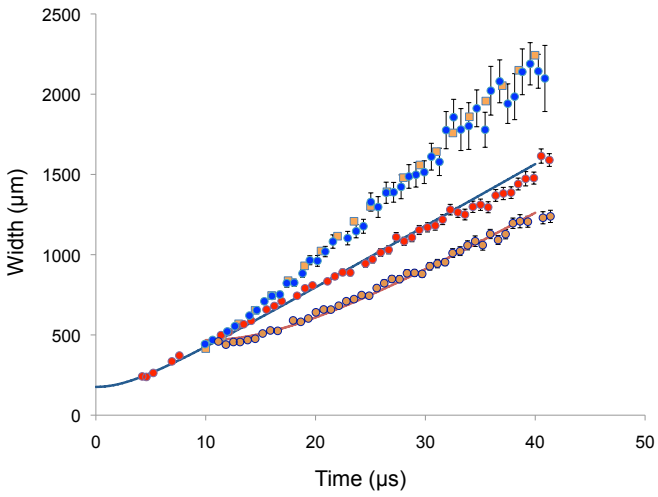

FIG. 3: (color online) Central trace: Electron RMS half-width, $\sigma(t)$, of the electron signal waveform measured for the plasma that evolves from a Rydberg gas created at position 1. Upper trace: $\sigma(t)$ of of the electron signal waveform measured for the plasma perturbed by injecting hot electrons at position 2 after an elapsed time, $t = 10$ μs. Square points obtained for a shell model of the concentric colliding plasmas (see text). Lower trace: $\sigma(t)$ of of the electron signal waveform measured for the plasma perturbed by injecting a secondary Rydberg gas with $n_0 = 60$ at position 2 after an elapsed time, $t = 10$ μs. Solid line represents a Vlasov expansion commencing at $t = 0$ μs for an electron temperature of 5 K.

Rydberg gas created at position 1. The plotted width begins to change slowly, then rises with a slope that reflects a ballistic radial ion velocity of 38 m s^{-1}. Previous work has shown that such a variation in width as a function of time for a simple laser-produced molecular beam plasma conforms reasonably with the Vlasov equations for a self-similar expansion of a quasi-neutral Gaussian distribution of ions and electrons [11, 16], much as observed in a MOT [1]:

$$\sigma_z(t) = \sigma_z(0)\left(1 + \frac{t^2}{\tau_z^2}\right)^{1/2} \qquad (1)$$

where $\sigma_z(0)$ describes the RMS radius of the plasma formed by initial evolution from the Rydberg gas, and τ_z is the characteristic time for radial expansion of the ions measured in z. This latter quantity is determined by thermal motion of the ions at an initial temperature $T_i(0)$ plus the hydrodynamic acceleration caused by electrostatic coupling to an expanding electron gas with initial temperature, $T_e(0)$:

$$\tau_z^2 = \frac{m_i \sigma_z(0)^2}{k_B\left[T_e(0) + T_i(0)\right]} \qquad (2)$$

The solid curve through the central data in Figure 3 plots $\sigma_z(t)$ predicted by the Vlasov equations for a self-similar expansion of a quasi-neutral Gaussian distribution of ions and electrons for $\sigma_z(0) = 176\pm2$ μm, $T_e = 5.4$ K and $T_i = 1$ K.

This conventional plasma formed by $\omega_1 + \omega_2$ double-resonant excitation, and its apparent self-similar expansion, provide a useful frame of reference from which to interpret the expansion behaviour of plasma volumes perturbed by $\omega_1' + \omega_2'$ secondary excitation.

Direct $\omega_1' + \omega_2'$ photoionization of residual NO in the excitation volume modifies the plasma state at $t = 10$ μs by adding a population of hot electrons. Figure 3 shows that this injection of energetic electrons at $t = 10$ μs does not immediately affect the expansion rate. But, between 15 and 20 μs, the ions accelerate to nearly double their radial velocity.

Tuning ω_2' to a Rydberg resonance initially freezes the plasma, decelerating the radial velocity nearly to zero. The ions then again begin to accelerate, eventually reaching a ballistic velocity comparable to that of the unperturbed plasma.

We can qualitatively explain these effects on physical grounds. Referring first to secondary excitation below threshold, we note that Pillet and coworkers have similarly added Rydberg atoms to an ultracold plasma in a caesium MOT, probing the effect on electron density and temperature [17]. Much like our results, they find that electron collisions rapidly ionize the added Rydberg gas, and that accompanying Rydberg redistribution acts to balance the associated energy cost, causing the temperature to remain about the same [18]. This then leaves only the inertial effect of the cold secondary ions, which, after a time, equilibrate with the expanding gas of electrons and primary ions.

The injection of hot electrons by direct photoionization supplies a source of energy that must increase the effective pressure of the electron gas on the radially accelerated ions. In this case as well, secondary excitation also adds the inertial mass of a new population of ions that have the sub-Kelvin temperature of the neutral molecules in the supersonic beam.

In an effort to account for this perturbation quantitatively, we have developed a hydrodynamic shell model for colliding plasmas, which we apply here to the particular case of above-threshold electron/ion injection. We assume that the electrons equilibrate instantaneously and form a neutralizing bath. The expansion of this electron gas entirely governs the dynamics of the ions, so we can treat the primary and secondary ion spatial distributions separately.

We describe these ion distributions as spherical Gaussians approximated by two sets of 200 concentric spherical shells. Each shell encloses a particular number of ions and neutralizing electrons. As the plasma expands, the shell boundaries grow to maintain a constant number of ions. Quasi-neutrality persists, but electrons and electron energy exchange rapidly between shells.

Figure 4 diagrams this situation. The larger system of shells defines a distribution of concentric volume elements, each containing a defined number of ions (and

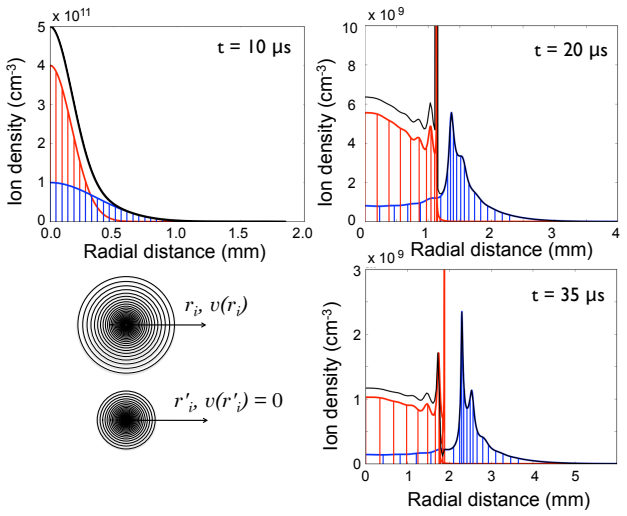

FIG. 4: (color online) Schematic diagram representing a shell model for the hydrodynamics of concentric cold-ion neutral plasmas undergoing ambipolar expansion. (lower left) Representation of shells for a primary plasma expanding with shell velocity, $v(r_i)$ determined by 10 μs of self-similar ambipolar expansion, and shells formed at $t = 10$ μs by secondary excitation. (upper left) Initial spherical Gaussian charge distributions for the primary plasma (blue) and the secondary plasma (red). (right) Charge distributions after 20 and 35 μs of expansion. In all cases, a black curve describes the electron charge distribution.

neutralizing electrons) at a succession of defined densities. We neglect the thermal motion of the cations, so each of these shells expands with an indexed velocity $v(r_i)$ that starts with all values of $v(r_i)$ equal to 0 at $t = 0$.

The narrower system of shells defines a separate distribution of concentric volume elements containing ions and electrons created at $t = 10$ μs by the laser pulse sequence $\omega_1' + \omega_2'$. At $t = 10$ μs, primary shell velocities, $v(r_i)$, have values that cause $d\sigma/dt$ to equal 38 μm μs, while all secondary shell velocities, $v(r_i')$, equal 0.

We treat each ion shell independently, calculating the distinct force acting upon it owing to the immediate gradient of the electronic density distribution. The first moment of the Boltzmann equation describes the potential that determines these expansion forces. With reference to the generalized velocity coordinate u, an ion in either the primary or secondary system, experiences an acceleration determined by:

$$\frac{du}{dt} = -\frac{e}{m_i}\nabla\phi \tag{3}$$

where $e\nabla\phi$ is the gradient of the electron density distribution at the radial position of the ion and m_i is the ion mass. In the limit of quasi-neutrality, an electron density distribution, defined by superimposed shells of uniform ion density, yields a gradient in terms of discrete differences:[19]

$$e\nabla\phi(r_i) = k_B T_e \frac{1}{n_e(r_i)} \frac{n_e(r_{i+1}) - n_e(r_{i-1})}{r_{i+1} - r_{i-1}} \tag{4}$$

where r_i refers to a shell radius in either system, and $n_e(r_i)$ is the local electron density determined by the total number of ions as a function of r_i.

As this system expands each shell moves with a radial velocity,

$$\frac{\partial r_i(t)}{\partial t} = u_i(t) = \gamma_i(t) r_i(t) \tag{5}$$

Neglecting loss by dissociation, the density change in each shell satisfies the continuity equation,

$$\frac{\partial n_i(t)}{\partial t} + \frac{n_i}{V_i(t)} \frac{\partial V_i(t)}{\partial t} = 0 \tag{6}$$

where V_i is the volume of shell i,

$$V_i = \frac{4}{3}\pi(r_{i+1}^3 - r_i^3) \tag{7}$$

and,

$$\frac{\partial V_i(t)}{\partial t} \approx 3\gamma_i(t) V_i(t) \tag{8}$$

The expansion of the electron gas accelerates the cations. Energy flows from the thermal motion of the electrons to the radial motion of the ions, and the electron temperature falls by an amount,

$$\frac{dT_e}{dt} = -\frac{2m_i}{3k_B N_e} \sum_i N_i u_i \frac{du_i}{dt} = \frac{2}{3k_B N_e} \sum_i N_i u_i e\nabla\phi(r_i) \tag{9}$$

Equations (3), (4) and (6) describing ion acceleration, together with (9) for the decrease in electron temperature, form a complete set for numerical integration to determine $r_i(t)$, $n_i(t)$ and $T_e(t)$. This system of shells and forces forms a fluid model for the expansion dynamics.

Figure 4 diagrams the initial conditions for a simulation that begins at $t = 10$ μs. At this point, self-similar expansion of the $\sigma(0) = 176$ μm plasma created at $t = 0$ extends to reach the RMS width observed experimentally, $\sigma(10) = 450$ μm. Within this volume, delayed photoionization produces a secondary plasma with a $\sigma'(10) = 170$ μm, determined by the diameter of ω_1'.

The primary ions have radial velocities described by the function $u = \gamma r$ for which $d\sigma/dt = 38$ μm μs^{-1}, the value fit experimentally to the unperturbed expansion. The secondary ions are assumed to be stationary at $t = 10$ μs. The systems of shells that describe the primary and secondary ion spatial distributions extend from the origin to values of r equal to five times the respective RMS width.

From the plasma electron signals plotted in Figure 2, we judge that the secondary plasma created by $\omega_1' + \omega_2'$

photoionization contains roughly the same number of electrons as the primary plasma. With ambipolar expansion of the primary ions having consumed most of the initial thermal energy of the primary electrons, we approximate the equilibrated electron temperature at $t = 10$ μs to be $T_e = 19$ K.

The expanding electron gas with this thermal energy now acts on the ions in the primary and secondary shell systems. We follow the consequences by numerically integrating Equations (3), (4), (6) and (9) for the initial conditions described above.

The inertia of the stationary ions in the secondary shell system slows the expansion of the electron gas. The established radial momentum of the primary ions opposes this retardation. This couples the radial motion of the primary ions to that of the secondary ions. Near ballistic motion of the outermost primary ions depletes the trailing charge distribution in the wings of the inner plasma. The resulting charge gradient reversal forms collisionless shock waves in the calculated primary and secondary ion charge distributions, as evident from the snapshots at $t = 20$ and 35 μs in Figure 4.

Killian and coworkers have observed similar effects as ion acoustic waves in plasmas prepared in a perturbed state by spatially patterned photoionization [20]. Molecular dynamics simulations of Pohl, Pattard and Rost predict shocks at the edge of a simple one-component plasma arising from deviations in quasi-neutrality not considered in our hydrodynamic model [21].

Two additional factors affect the experimental observability of such shocks in a molecular system. Our model makes no provision for the dissociative recombination (DR) of NO^+ with electrons [16, 19], or for that matter, three-body recombination of ions and electrons, which can be expected to limit the density of shock structures in atomic as well as molecular plasmas.

Secondly, as the plasma propagates in z at the velocity of our molecular beam, we detect its electron density as a z projection of the signal integrated over x and y, sampled by its transit through the perpendicular grid, G_2 (see Figure 1).

The corresponding experimental waveforms calculated from the radial distributions predicted by our fluid model yield a width as a function of time, but average away the fine structure of the simulated shocks. The square points in Figure 3 plot the widths predicted in this way for the parameters considered above. These agree well with results observed experimentally, including an inertial lag in ion acceleration.

Thus, using photoionization to inject a secondary plasma of NO^+ ions and energetic electrons increases the expansion rate of a primary ultracold plasma. Introducing instead a secondary Rydberg gas slightly diminishes the terminal velocity of the plasma ions. In both cases, we see an interval of time during which the inertial drag of the cold secondary ions retards the thermal expansion of the electron gas. We can account for these effects in terms of a cold-ion shell model for the ambipolar hydrodynamics. This model accounts well for the overall effect of energy added by photoionization electrons.

This work was supported by the US Air Force Office of Scientific Research (Grant No. FA9550-12-1-0239), together with the Natural Sciences and Engineering research Council of Canada (NSERC), the Canada Foundation for Innovation (CFI) and the British Columbia Knowledge Development Fund (BCKDF).

[1] S. Laha, P. Gupta, C. E. Simien, H. Gao, J. Castro, T. Pohl, and T. C. Killian, Phys. Rev. Lett. **99**, 155001 (2007).
[2] M. Perego, P. D. Howell, M. D. Gunzburger, J. R. Ockendon, and J. E. Allen, Physics of Plasmas **20**, 052101 (2013).
[3] G. Sarri, M. E. Dieckmann, I. Kourakis, and M. Borghesi, Phys Rev Lett **107**, 025003 (2011).
[4] A. E. Kaplan, B. Y. Dubetsky, and P. L. Shkolnikov, Phys Rev Lett **91**, 143401 (2003).
[5] Y. Kuramitsu, Y. Sakawa, T. Morita, C. D. Gregory, J. N. Waugh, S. Dono, H. Aoki, H. Tanji, M. Koenig, N. Woolsey, et al., Phys Rev Lett **106**, 175002 (2011).
[6] A. Stockem, F. Fiuza, A. Bret, R. A. Fonseca, and L. O. Silva, Scientific Reports **4** (2014).
[7] P. Gupta, S. Laha, C. E. Simien, H. Gao, J. Castro, T. C. Killian, and T. Pohl, Phys. Rev. Lett. **99**, 075005 (2007).
[8] T. Killian, T. Pattard, T. Pohl, and J. Rost, Physics Reports **449**, 77 (2007).
[9] J. P. Morrison, C. J. Rennick, J. S. Keller, and E. R. Grant, Phys. Rev. Lett. **101**, 205005 (2008).
[10] J. P. Morrison, C. J. Rennick, and E. R. Grant, Phys. Rev. A **79**, 062706 (2009).
[11] N. Saquet, J. P. Morrison, M. Schulz-Weiling, H. Sadeghi, J. Yiu, C. J. Rennick, and E. R. Grant, J Phys B **44**, 184015 (2011).
[12] H. Sadeghi, A. Kruyen, J. Hung, J. H. Gurian, J. P. Morrison, M. Schulz-Weiling, N. Saquet, C. J. Rennick, and E. R. Grant, Phys Rev Lett **112**, 075001 (2014).
[13] S. G. Kuzmin and T. M. O'Neil, Phys. Rev. Lett. **88**, 065003 (2002).
[14] K. Niffenegger, K. A. Gilmore, and F. Robicheaux, J. Phys. B **44**, 145701 (2011).
[15] J. Hung, H. Sadeghi, M. Schluz-Weiling, and E. Grant, J Phys B **47**, 155301 (2014).
[16] H. Sadeghi, M. Schulz-Weiling, J. P. Morrison, J. C. H. Yiu, N. Saquet, C. J. Rennick, and E. Grant, Phys. Chem. Chem. Phys. **13**, 18872 (2011).
[17] N. Vanhaecke, D. Comparat, D. A. Tate, and P. Pillet, Phys Rev A **71**, 013416 (2005).
[18] T. Pohl, D. Comparat, T. Zahzam, T. Vogt, P. Pillet, and T. Pattard, Eur Phys J D **40**, 45 (2006).
[19] H. Sadeghi and E. R. Grant, Physical Review A **86**, 052701 (2012).
[20] J. Castro, P. McQuillen, and T. C. Killian, Phys Rev Lett **105**, 065004 (2010).

[21] T. Pohl, T. Pattard, and J. M. Rost, Phys Rev A **70**, 033416 (2004).